

Sub-barrier quasifission in heavy element formation reactions with deformed actinide target nucleiD. J. Hinde,^{*} D. Y. Jeung, E. Prasad,[†] A. Wakhle,[‡] M. Dasgupta, M. Evers,[§] D. H. Luong,^{||} R. du Rietz,[¶] C. Simenel, E. C. Simpson, and E. Williams*Department of Nuclear Physics, Research School of Physics and Engineering, The Australian National University, Canberra, ACT 2601, Australia*

(Received 15 November 2017; published 23 February 2018)

Background: The formation of superheavy elements (SHEs) by fusion of two massive nuclei is severely inhibited by the competing quasifission process. Low excitation energies favor SHE survival against fusion-fission competition. In “cold” fusion with spherical target nuclei near ^{208}Pb , SHE yields are largest at beam energies significantly below the average capture barrier. In “hot” fusion with statically deformed actinide nuclei, this is not the case. Here the elongated deformation-aligned configurations in sub-barrier capture reactions inhibits fusion (formation of a compact compound nucleus), instead favoring rapid reseparation through quasifission.

Purpose: To determine the probabilities of fast and slow quasifission in reactions with prolate statically deformed actinide nuclei, through measurement and quantitative analysis of the dependence of quasifission characteristics at beam energies spanning the average capture barrier energy.

Methods: The Australian National University Heavy Ion Accelerator Facility and CUBE fission spectrometer have been used to measure fission and quasifission mass and angle distributions for reactions with projectiles from C to S, bombarding Th and U target nuclei.

Results: Mass-asymmetric quasifission occurring on a fast time scale, associated with collisions with the tips of the prolate actinide nuclei, shows a rapid increase in probability with increasing projectile charge, the transition being centered around projectile atomic number $Z_p = 14$. For mass-symmetric fission events, deviations of angular anisotropies from expectations for fusion fission, indicating a component of slower quasifission, suggest a similar transition, but centered around $Z_p \sim 8$.

Conclusions: Collisions with the tips of statically deformed prolate actinide nuclei show evidence for two distinct quasifission processes of different time scales. Their probabilities both increase rapidly with the projectile charge. The probability of fusion can be severely suppressed by these two quasifission processes, since the sub-barrier heavy element yield is likely to be determined by the *product* of the probabilities of surviving each quasifission process.

DOI: [10.1103/PhysRevC.97.024616](https://doi.org/10.1103/PhysRevC.97.024616)**I. INTRODUCTION**

Superheavy nuclei—isotopes of elements with atomic number $Z \geq 104$ —are created in the laboratory by fusion of two heavy nuclei. There are three sequential processes involved in superheavy element (SHE) synthesis by fusion followed by neutron evaporation. The fastest is capture, where the two nuclear surfaces “stick” together. This is followed by shape

evolution to form a compact compound nucleus, and finally survival as an evaporation residue (ER) against statistical fission decay. Because of the different typical time scales of each process, the cross section for heavy element formation is written as the product of factors related to the three stages of formation:

$$\sigma_{ER} = \sum_{J=0}^{\infty} \sigma_J(E_{c.m.}, J) P_{CN}(E_x, J) W_{sur}(E_x, J). \quad (1)$$

Here $\sigma_J(E_{c.m.}, J)$ is the capture cross section as a function of center-of-mass energy $E_{c.m.}$ and angular momentum $J\hbar$. It is the fastest process, occurring in $\sim 10^{-21}$ s. $P_{CN}(E_x, J)$ is the probability that the system reaches the compact compound nucleus equilibrium configuration, expressed as a function of the excitation energy E_x and J . P_{CN} can reduce SHE cross sections by several orders of magnitude, through the separation of the system formed after capture into two fissionlike fragments (quasifission) on a time scale of $\sim 10^{-20}$ s [1–4]. For fusion reactions forming much lighter nuclei, $P_{CN} = 1$, and thus capture and fusion need not be distinguished. $W_{sur}(E_x, J)$ is the probability that the system survives statistical fission decay through sequential particle evaporation, thus eventually

^{*}Corresponding author: david.hinde@anu.edu.au[†]Present address: Department of Physics, School of Mathematical and Physical Sciences, Central University of Kerala, Kasaragod 671314, India.[‡]Present address: Cyclotron Institute, Texas A&M University, College Station, Texas 77843, USA.[§]Present address: ACRF Department of Cancer Biology and Therapeutics, The John Curtin School of Medical Research, The Australian National University, Canberra, ACT 2601, Australia.^{||}Present address: Scandinavian Health Limited, Taiwan Branch, 136 Guosheng 2nd Street, Taoyuan District, Taoyuan City 330, Taiwan.[¶]Present address: Malmö University, Faculty of Technology and Society, Malmö 205 06, Sweden.

forming the desired (super)heavy evaporation residue. In near-barrier superheavy element formation reactions, this time scale is typically $\gg 10^{-20}$ s, and according to the Bohr independence hypothesis, $W_{\text{sur}}(E_x, J)$ should be independent of the two nuclei that have fused. Crucially, low excitation energies are expected to maximize $W_{\text{sur}}(E_x, J)$ through reducing the probability of multichance statistical fission following formation of a compact compound nucleus.

The successful formation of superheavy nuclei is a delicate balance. On the one hand, fission competition is minimized by low E_x , which can be achieved by using heavy projectiles. On the other hand, quasifission should be minimized (and thus P_{CN} maximized) by minimizing the charge product of the two colliding nuclei [5]. This can be achieved by using light projectiles, but results in higher E_x . This situation has resulted in two rather different methods that have been successful in SHE synthesis, namely “cold fusion” and “hot fusion” reactions, which are described below.

A. Cold fusion

Cold fusion [6–9] uses target nuclei close to the doubly-magic nucleus ^{208}Pb . It has been successful in forming elements up to $Z = 113$ through fusion reactions with projectiles from Ti ($Z = 22$) to Zn ($Z = 30$). The large binding energy associated with the magic proton number $Z = 82$ and neutron number $N = 126$ can result in the formation of superheavy nuclei with extremely low E_x , which is the reason that this fusion pathway is called cold fusion.

For survival against fusion-fission competition, expressed through $W_{\text{sur}}(E_x, J)$, cold fusion reactions should be favorable for superheavy element formation. However, the probability P_{CN} of reaching a compact, fully equilibrated compound nucleus can be severely reduced by quasifission. The rapid reseparation of the system, before reaching the compact fused configurations, can result in very small $P_{\text{CN}}(E_x, J)$ values, suppressing fusion by many orders of magnitude [10].

The quasifission probability increases strongly with the charge product of the projectile and target nuclei. In forming SHE heavier than Cn ($Z = 112$), this is the major disadvantage of using target nuclei close to ^{208}Pb . Here it is advantageous to use lighter projectile nuclei bombarding heavier (actinide) target nuclei, in the “hot fusion” process described below.

B. Hot fusion

Hot fusion [7, 11–13] uses actinide target nuclei, generally uranium ($Z = 92$) and heavier, thus reducing the charge product in the entrance channel. The disadvantage of this pathway is that for reactions at the capture barrier energy, the excitation energy of the compound nucleus is considerably greater than in cold fusion. This will result in a higher probability of fission of the compact compound nucleus than in cold fusion. However, the more neutron-rich target nuclei, combined with the use of the very neutron-rich projectile ^{48}Ca , allows the formation of more neutron-rich compound nuclei than in cold fusion. This should counteract to some extent the effect of higher excitation energy on the fission probability. It has been found that hot fusion with ^{48}Ca results in a quasifission probability that is

small enough (and thus P_{CN} is large enough) to more than compensate for the expected lower fission survival probability W_{sur} . Hot fusion reactions in which ^{48}Ca has bombarded target nuclei of elements up to Cf have allowed creation and identification [11–14] of elements up to $Z = 118$ (Oganesson) [15]. There is currently insufficient material of any element heavier than Cf to make targets to allow the synthesis of still heavier elements using ^{48}Ca beams. Thus using beams of heavier elements is currently the only option.

To understand and predict the formation cross sections for superheavy elements covering a wide range of projectile-target combinations, the dependence of $P_{\text{CN}}(E_x, J)$ and $W_{\text{sur}}(E_x, J)$ on all the variables associated with different projectile-target combinations and beam energies should be explicitly modelled. These include not only macroscopic quantities such as entrance channel charge product, compound nucleus fissility, and excitation energy, but also the influence of the nuclear structure of the projectile and target nuclei, and the compound nucleus.

In the case of the latter, it is proposed [15] that the unexpectedly large cross sections for elements in the range 114–118 is evidence for shell effects increasing the fission barrier heights, and thus for the proximity of these nuclides to the island of stability. How these shell effects vary with neutron number for a given element will affect the values of $W_{\text{sur}}(E_x, J)$, and thus influence the possibilities for success with different reactions populating less or more neutron-rich isotopes. However, shell structures of the two colliding nuclei can also have very important effects, through their influence on P_{CN} , as discussed below.

C. Nuclear structure and the competition between quasifission and fusion

Experimental studies of quasifission characteristics [16, 17] have clearly shown that effects of shell structure of the colliding nuclei affects the competition between fusion and quasifission (and thus on P_{CN}). This is discussed below, first for spherical magic nuclei, and then for heavy statically deformed nuclei.

1. Spherical magic numbers

As well as neutron richness and a relatively low atomic number, the doubly magic nature of the ^{48}Ca nuclei used in hot fusion appears to help during the fusion process. The competition between fusion and quasifission at near- and below-barrier energies is expected to be affected by spherical shells, which results in so-called “cold valleys” in the potential energy surface, which provides a pathway to a compact compound nucleus [18, 19]. Another possible mechanism resulting in an increased P_{CN} comes from the reduced kinetic energy dissipation expected in these valleys [7, 19, 20]. Measurements [17] of quasifission characteristics at sub-barrier energies have been reported in collisions of nuclei close to ^{48}Ca with nuclei close to ^{208}Pb . The results showed strong evidence that the presence of *several* magic numbers, together with matching of the N/Z values of the two colliding nuclei, can be important at near-barrier energies in assisting two heavy nuclei to fuse to form a compact compound nucleus.

In contrast, an analysis [20] of fusion-evaporation residue yields at higher E_x (above the average capture barrier) demonstrated that a *single* magic number (whether in the projectile or the target nucleus) has little effect on heavy element yields. Thus the quantitative effect of the doubly magic nature of ^{48}Ca in hot fusion reactions with (nonmagic) actinide nuclei is not yet clear. However, it is clear that the static deformation of these actinide nuclei does play an important role.

2. Static deformation alignment

The nuclear structure (dominantly the static prolate shape) of the actinide collision partners in hot fusion is understood to play a significant role in capture. This is associated with the orientation of the deformation axis with respect to the contact point of the lighter projectile nucleus [21]. This effect has been demonstrated in reactions with rare-earth deformed nuclei from as long ago as 1978 [22–28].

It is expected, and has been shown in time-dependent Hartree-Fock (TDHF) calculations [29–32] of heavy element formation reactions, that radial motion is rapidly damped after the nuclear surfaces make contact. This means that when contact occurs close to the tip of the prolate target nucleus, the configuration of the dinuclear system that is initially formed is very elongated. In contrast, the configuration is much more compact where contact occurs close to the short axis (equator) of the deformed actinide nucleus.

In hot fusion reactions, the capture barrier energy depends on the angle between the prolate target nucleus deformation axis with the line joining the centers of the two nuclei at the distance where capture is decided [21]. The large static prolate deformation of actinide nuclei [33] means that in the deformation-aligned configuration (also known as axial or tip collisions), capture can occur at collision energies significantly below the average barrier energy, resulting in much lower excitation energies and larger $W_{\text{sur}}(E_x, J)$ than collisions at the barrier. This effect by itself would favor sub-barrier collisions to synthesize SHEs. However, the effect on P_{CN} must also be considered, in view of the compactness or elongation of the contact configuration.

The importance of the concept of compactness on the fusion dynamics was first expressed in theoretical consideration of collisions of two deformed tungsten nuclei with different relative orientations, resulting in the term “hugging fusion” [34]. The first experimental phenomenon attributed to the effects of deformation alignment was the increase in fission angular anisotropies found with decreasing beam energy through the average fusion barrier energy for the reaction $^{16}\text{O} + ^{238}\text{U}$ [35,36]. It was suggested then (more than 20 years ago) that these results should mean that quasifission would be more likely for the elongated deformation aligned configuration (with suppression of fusion shown experimentally in Refs. [37,38]), and conversely inhibited for reactions in the equatorial configuration, favoring heavy element formation [36]. As far as we know, the suggestion of *enhancement* of compound nucleus formation in equatorial configurations [35] has not yet been proven experimentally, but seems reasonable, and is supported by TDHF calculations [31,39]. The quantitative determination of $P_{\text{CN}}(E_x, J)$ for different projectiles and

alignment angles of the deformation axis is of general importance to predict optimum reactions to form new superheavy elements and isotopes, and is the subject of this work.

3. New prospects

It has recently been suggested [40] based on Langevin dynamics calculations of mass distributions matched to experimental data, that production of SHEs in collisions at sub-barrier energies might yet be a feasible approach to SHE production. It would be desirable to investigate experimentally in more detail the dynamics of sub-barrier reactions, to provide more quantitative experimental data to test models, and allow more reliable predictions.

Here we present experimental measurements of mass and angular distributions, and a phenomenological analysis that throws light on sub-barrier quasifission probabilities in reactions with prolate deformed actinide nuclei.

II. EXPERIMENTAL DETAILS

Measurements of mass-angle distributions and of angular anisotropies were carried out in separate experiments at the Australian National University Heavy Ion Accelerator Facility, using the 14UD electrostatic tandem accelerator.

Beams ranging in mass from ^{12}C to ^{34}S bombarded targets of ^{232}Th and ^{238}U . Beam energies typically ranged from 8% below to 10% above the fusion barrier energies for each reaction.

Reaction products were detected using the CUBE spectrometer [5,36,41], consisting of two large area (279 mm \times 357 mm active area) position sensitive multiwire proportional counters (MWPCs). The detectors were placed with their normal 180 mm from the target. A schematic view of the experimental configurations used is given in Fig. 1 of Ref. [41], and full experimental details are also given there.

Target thicknesses ranged from a few tens to a few hundred $\mu\text{g}/\text{cm}^2$. The $^{\text{nat}}\text{UF}_4$ targets were evaporated onto $\sim 25 \mu\text{g}/\text{cm}^2$ carbon backings, while the $^{\text{nat}}\text{Th}$ targets were supported by similar carbon backings or $\sim 50 \mu\text{g}/\text{cm}^2$ aluminium. The target normal was oriented at 60° to the beam axis for mass-angle distribution measurements (detector configuration *A* of Ref. [5]), and at 45° for angular anisotropy measurements (configuration *B* of Ref. [5]). The target backings faced downstream, and together with the chosen target orientations, minimized the effects of energy loss of fission fragments in the targets. In the analysis, energy loss corrections were applied iteratively, event by event, to the energy of the beam particles and the detected fission fragments assuming interactions occurred at the center of the actinide layer.

Pulsed beams were used, with a pulse full width at half maximum (FWHM) of 0.7–1.5 ns, and a pulse separation of 107 ns. The pulsed beams allowed event-by-event determination of the components of the fissioning nucleus velocity vector, both parallel to the beam (v_{\parallel}) and perpendicular to it (v_{\perp}) as described in Ref. [36]. This allowed optimal separation of fission following capture of the full projectile mass, known as full momentum transfer (FMT) fission—the process of interest—from fission of excited targetlike nuclei. These can result from transfer of a few or many nucleons, leaving the targetlike nucleus excited above the energy of its fission barrier.

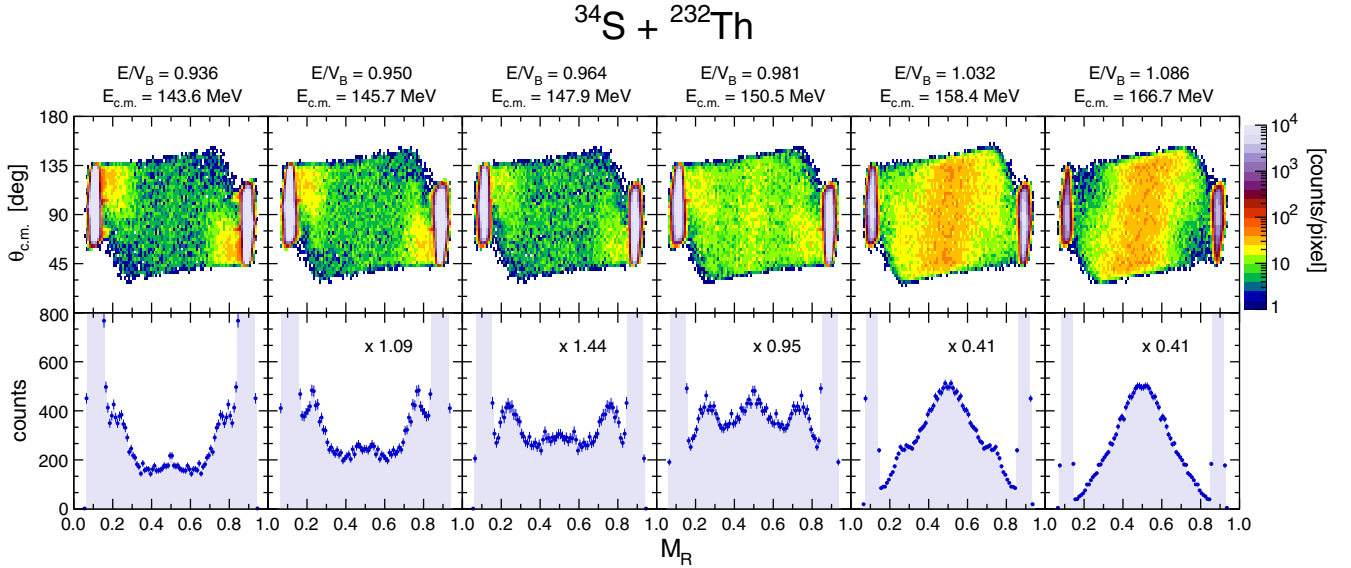


FIG. 1. The upper panels show the measured mass-angle distributions of FMT events for the reaction $^{34}\text{S} + ^{232}\text{Th}$, forming ^{266}Sg , at the indicated center-of-mass bombarding energy $E_{c.m.}$. The ratio E/V_B (independent of the reference frame) is also given, where the average barrier energy V_B is 153.5 MeV in the c.m. frame. The intensity scale is counts, proportional to $d^2\sigma/d\theta dM_R$. The lower panels show the projected mass-ratio (M_R) spectra for the angular range $45^\circ < \theta_{c.m.} < 135^\circ$. The counts have been multiplied by the indicated scale factors. A transition occurs from predominantly mass-asymmetric quasifission at sub-barrier energies to apparently mass-symmetric fission at $E > V_B$. The MADs show that the mass-asymmetric component has a very fast time scale, while the component peaked at symmetry shows a significant mass-angle correlation, inconsistent with fusion fission.

III. EXPERIMENTAL RESULTS AND ANALYSIS

First the experimental trends will be presented, with a qualitative interpretation. An evaluation of the detection efficiency as a function of mass ratio is then given, which allows a quantitative analysis of the experimental results. This permits *quantitative* information on quasifission probabilities to be determined directly from experimental data, carrying important information on fusion and quasifission dynamics.

A. Mass-angle distributions

Mass-angle distributions (MADs) with complete coverage in $\theta_{c.m.}$ from 45° to 135° were measured for four reactions. The compound nucleus ^{266}Sg was formed using the reactions $^{28}\text{Si} + ^{238}\text{U}$ and $^{34}\text{S} + ^{232}\text{Th}$. Similarly, two reactions were used to form the lighter nuclide ^{262}Rf , namely $^{24}\text{Mg} + ^{238}\text{U}$ and $^{30}\text{Si} + ^{232}\text{Th}$. As described in Refs. [5,36], mass-angle distributions for FMT fission (including both fusion fission and quasifission) were determined. Except at the detector edges, the azimuthal angle coverage of the detector system was independent of scattering angle. Thus the number of counts at a given point on the MAD is directly proportional to the double differential cross section $d^2\sigma/d\theta dM_R$.

1. The $^{34}\text{S} + ^{232}\text{Th}$ reaction

MADs measured for the $^{34}\text{S} + ^{232}\text{Th}$ reaction have already been presented and extensively discussed in Ref. [42]. There, the clear separation of FMT fission and fission following transfer reactions was demonstrated (using v_{\parallel} and v_{\perp} [5,36]) for each beam energy. That work focused on extraction of

the time scales of quasifission from the angular information in the MADs. We focus here on the different yields and characteristics of the mass-asymmetric and mass-symmetric components, to obtain information on absolute quasifission probabilities.

Mass-angle distributions at six beam energies spanning the respective capture barrier energies are shown for $^{34}\text{S} + ^{232}\text{Th}$ in Fig. 1. The lower panels show the projected mass-ratio spectra from 45° to 135° . The beam energy with respect to the average capture barrier energy (E/V_B) is indicated for each measurement.

The intense mass-asymmetric quasifission component, seen most clearly at the lowest energies, results from fast re-separation after capture, giving rise to a memory of the entrance channel masses and angles. As the beam energy increases, a component peaked at mass-symmetry becomes more significant. The evolution of the relative yields of the mass-asymmetric and mass-symmetric components with beam energy is clearly seen from their respective M_R projections. In similar reactions, this changing pattern of the MADs with beam energy was seen for $^{32}\text{S} + ^{232}\text{Th}$ [16] (with lower statistics than the present data) and also in mass distributions measured over a narrower angular range for the $^{36}\text{S} + ^{238}\text{U}$ [43,44] reaction. This behavior has also been seen in the mass distributions for reactions of other projectiles bombarding actinide targets [39,40,44–46].

The beam energy dependence from below to above the capture barrier is explained qualitatively in terms of the deformation alignment [36,43,47] of the prolate target nuclei used in these reactions. At energies below the capture barrier, axial collisions (with the tips of the deformed target nucleus) are

dominant, since the capture barrier is lowest in this deformation aligned configuration [21]. As the elongation is far outside the unconditional saddle point [48], the system reseparates soon after capture, without much mass equilibration, leading to mass-asymmetric quasifission.

For equatorial collisions, which make the predominant contribution at $E/V_B > 1$, the contact configuration is more compact, resulting in a longer sticking time, and more complete mass equilibration [16,36]. TDHF calculations for the $^{40}\text{Ca} + ^{238}\text{U}$ reaction [30,39] have provided theoretical support for these scenarios.

The above-barrier M_R distributions show that the fission component centered on mass symmetry is wider than expected for fusion fission, and at above-barrier energies the MADs clearly exhibit a mass-angle correlation. Together with angular distributions (see Sec. III C), these observables all signal that the fission component centered at symmetry has a significant quasifission contribution. Langevin calculations for similar reactions also show quasifission events contributing to the mass-symmetric component [49].

2. The $^{28,30}\text{Si}$ and ^{24}Mg induced reactions

Having established the qualitative features of the MAD and mass distributions for the $^{34}\text{S} + ^{232}\text{Th}$ reaction, the results for the second reaction forming ^{266}Sg ($^{28}\text{Si} + ^{238}\text{U}$, shown in Fig. 2) are now compared. These show qualitatively the same features, also displaying clear mass-angle correlations. At the lowest energies the angle at which the mass-asymmetric group is centered is very similar, indicating that the time scale of these fast quasifission events is very similar to those for the $^{34}\text{S} + ^{232}\text{Th}$ reaction [42]. However, the relative yield of mass-asymmetric quasifission is lower, and the overall width of the mass distribution at the highest energies is clearly reduced.

Turning to the two reactions forming the lighter nuclide ^{262}Rf , the results for $^{30}\text{Si} + ^{232}\text{Th}$ are presented in Fig. 3. The overall features are very similar to the $^{28}\text{Si} + ^{238}\text{U}$ reaction, despite the reduction in the total charge of the system by 2. This indicates that the reduction in the projectile charge from 16 to 14 is the main reason for the observed differences between the ^{34}S and ^{28}Si reactions forming ^{266}Sg .

This conclusion is supported by the results for $^{24}\text{Mg} + ^{238}\text{U}$, also forming ^{262}Rf , which are shown in Fig. 4. Here the lower Z of 12 results in mass spectra more strongly peaked at symmetry (see also Fig. 5). The fission component centered at mass symmetry is dominant from below to above-barrier energies, and the MAD shows a reduced correlation with angle. Nevertheless at the highest energies shown ($E/V_B = 1.06, 1.08$) there is clear evidence of a correlation. This indicates that despite the equatorial collisions having a longer time scale than the axial collisions discussed above, some fraction of events have a time scale less than half a rotation, leading to a “memory” of the projectile mass and direction.

At lower beam energies, and thus angular momenta, the correlation with angle of the mass of the peak centered at symmetry is less clear, suggesting longer time-scale quasifission, and/or a higher probability of fusion fission. The presence of both mass-symmetric quasifission and fusion fission can be investigated using experimental angular anisotropies [41]. This will be addressed later in this paper.

At the two lowest energies, a weak mass-asymmetric component is seen at extreme backward and forward angles, in the same location as the group of fast quasifission events seen for the $^{28,30}\text{Si}$ and (with increased probability) ^{34}S -induced reactions. This result confirms the previous indication that Mg-induced reactions on actinide target nuclei do show a small component of mass-asymmetric quasifission [44].

Having made a qualitative survey of the experimental MADs as a function of beam energy, projectile charge, and

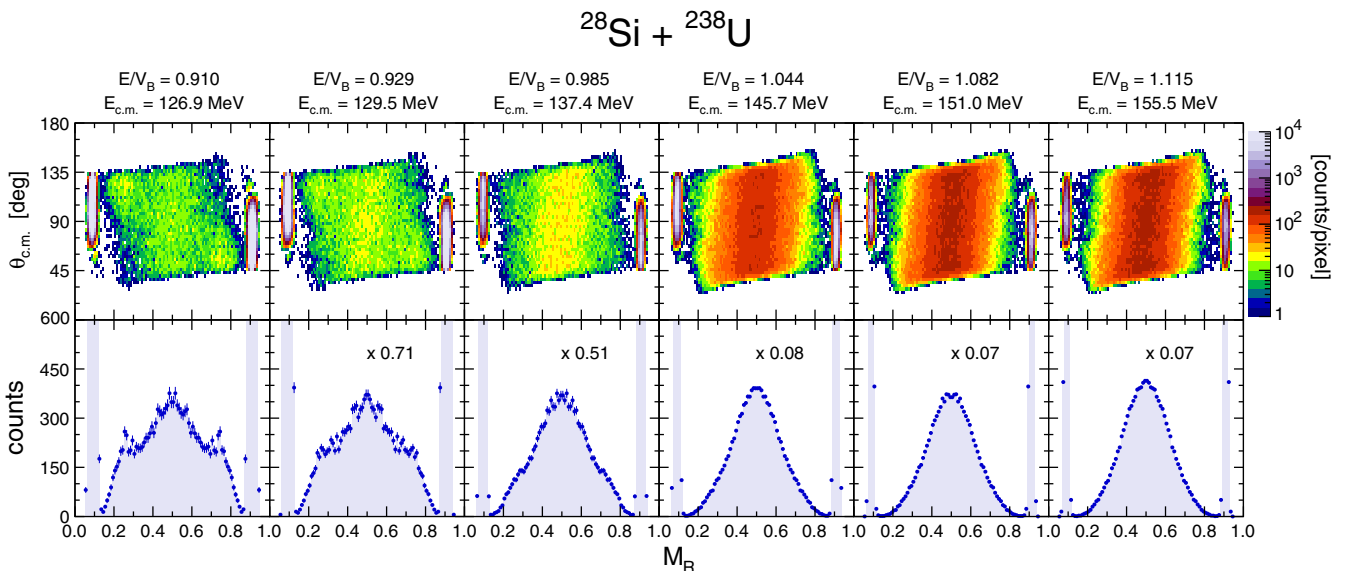


FIG. 2. As in Fig. 1 for the reaction $^{28}\text{Si} + ^{238}\text{U}$, also forming ^{266}Sg . The average barrier energy V_B was taken as 139.5 MeV. The mass-asymmetric quasifission component is weaker in this reaction.

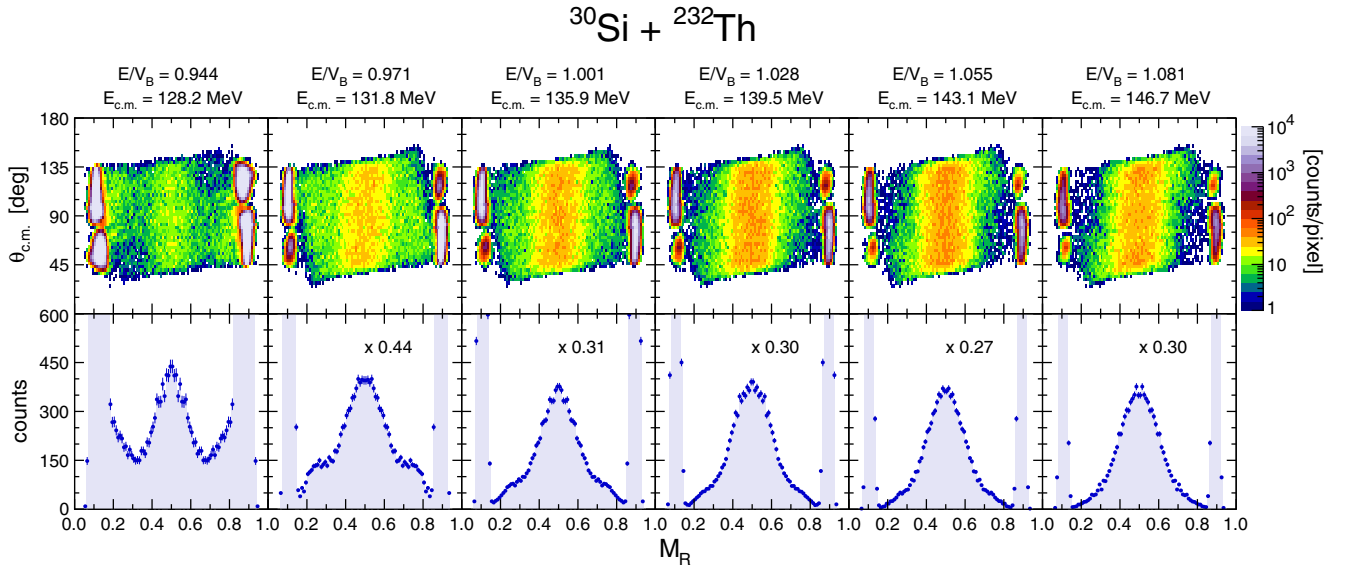


FIG. 3. As in Fig. 1 for the reaction $^{30}\text{Si} + ^{232}\text{Th}$, forming ^{262}Rf . The average barrier energy V_B was taken as 135.7 MeV. The mass-angle correlation of the mass-symmetric component is weaker in the reactions forming ^{262}Rf .

compound nucleus, it is clear that there is a systematic behavior as a function of all these variables. We will now make a quantitative determination of fast quasifission probabilities for each reaction, based on the observed energy dependence of the mass-ratio distributions.

B. Energy dependence of mass distributions

1. RMS of mass distributions

Symmetric-peaked fission mass distributions are often characterized by the standard deviation σ of a Gaussian fit. This is not appropriate for these mass distributions, which consist of

mass-symmetric and mass-asymmetric components. However, the root-mean-square (RMS) deviation of the fissionlike events can sensibly be evaluated independent of the shape of the mass-split distribution. The RMS deviation of the (symmetrized) distributions from 45° to 135° (for M_R from 0.17 to 0.83) are shown in Fig. 5 as a function of beam energy with respect to the capture barrier energy for each reaction. For this cut in M_R , the maximum possible RMS value is 0.33, and the experimental results lie between this value and the typical values for fusion fission of 0.07 [17,36,50]. The results for each reaction show a smooth dependence on E/V_B , giving confidence in the reliability of the measurements.

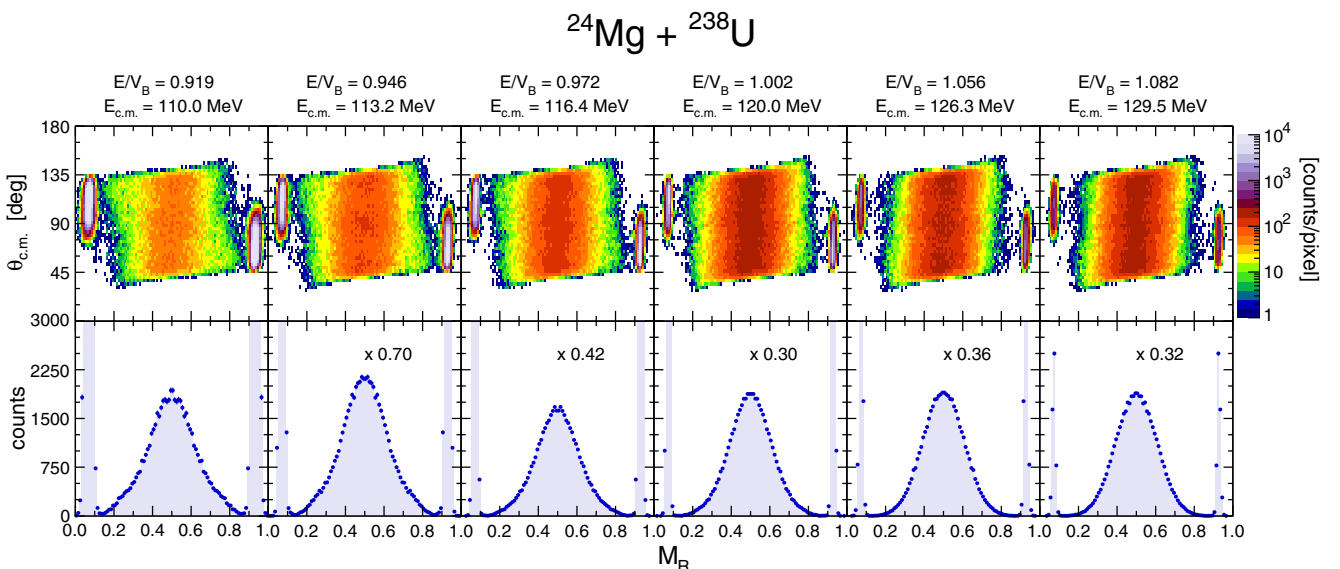


FIG. 4. As in Fig. 1 for the reaction $^{24}\text{Mg} + ^{238}\text{U}$, forming ^{262}Rf . The average barrier energy V_B was taken as 119.7 MeV. The mass-asymmetric quasifission component is weaker than in the $^{30}\text{Si} + ^{232}\text{Th}$ reaction forming ^{262}Rf .

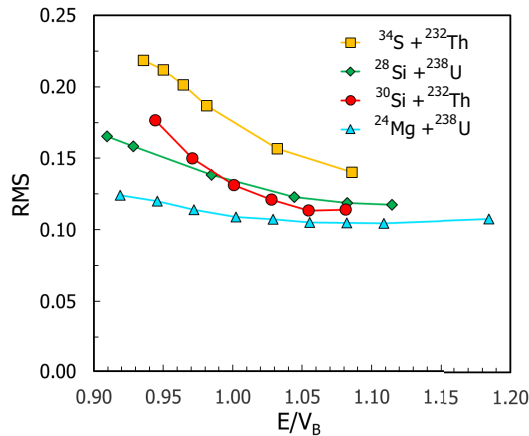


FIG. 5. The root-mean-square (RMS) value of the M_R spectra for all four reactions evaluated over the range $0.17 < M_R < 0.83$. They are plotted as a function of E/V_B . The expectation for fusion fission is approximately 0.07. The results show a smooth energy dependence, and are correlated strongly with the atomic number of the projectile Z_p and with E/V_B .

The RMS values are consistent with the overall conclusions from the MAD and mass-ratio spectra already discussed, with the $^{24}\text{Mg} + ^{238}\text{U}$ reaction having the smallest widths at all energies, the two Si-induced reactions having intermediate widths, and the S-induced reaction showing the largest RMS widths at all energies. Before making a quantitative interpretation of the ratios of mass-asymmetric to mass-symmetric fission from these measurements, the effect of the finite detector angular coverage must be accounted for.

2. Correction for detector angular coverage

The measured mass-ratio spectra represent only the center-of-mass frame angular region that the experiment covered fully, namely 45° to 135° . With a much narrower angular range, the results could change significantly, especially at the lowest energies, where the MADs show that the mass-asymmetric yields for angles close to 90° would be severely reduced. Equally, the results could change with a wider angular coverage (though to a lesser extent where the angular coverage is already large).

Because the current measurements cover a wide angular range, it is possible to estimate the yield in the missing angular region by using a model of quasifission mass-angle distributions fitted to the experimental results. This model was described and used in Refs. [4,5,42]. In the latter work, sets of sticking time and mass-evolution parameters were established that describe the mass and angular dependence of the quasifission yields for $^{34}\text{S} + ^{232}\text{Th}$. These were applied to all the reactions presented in this work (using the “mass-halt” scenario [42]), to estimate the mass yield in those angular regions not covered by the measurements. The relevant angular momentum distributions for capture were obtained from coupled-channels calculations including channel couplings as described in Ref. [42].

Figure 6 shows MADs for the $^{34}\text{S} + ^{232}\text{Th}$ reaction at three energies spanning the capture barrier. The measured MADs

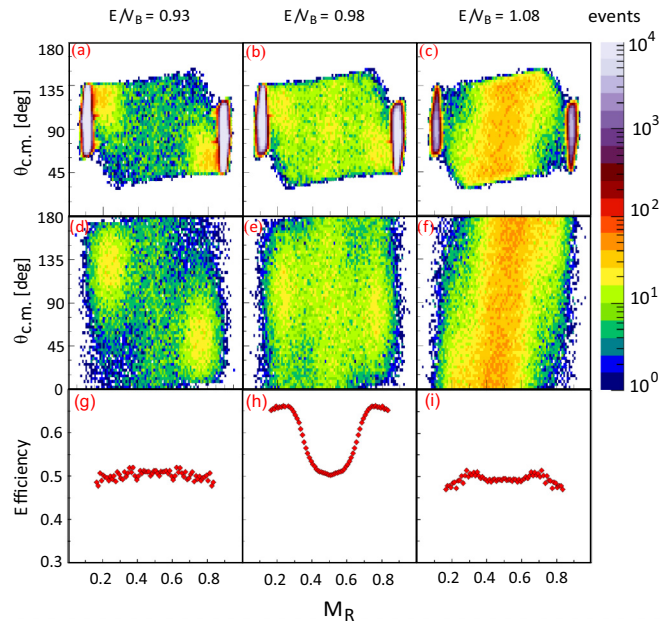


FIG. 6. Representative measured mass-angle distributions for the $^{34}\text{S} + ^{232}\text{Th}$ reaction at below-, near- and above-barrier energies in panels (a)–(c) respectively. Simulations including separate components for axial (tip) collisions and equatorial collisions are shown in panels (d)–(f). Simulation parameters were adjusted to give a good representation of the measurements over the experimentally measured coverage (see text). Panels (g)–(i) show the ratio of the simulated events in the experimental angular range to the total, thus providing the detection efficiency for a given mass ratio. At the near-barrier energy the fast mass-asymmetric quasifission events are peaked within the detector coverage, giving a high efficiency.

are shown in panels (a)–(c), and the corresponding Monte Carlo simulations in panels (d)–(f). The simulations give a good representation of the experimental data, and show how the quasifission yields may be extrapolated to 0° and 180° with a physically based model of quasifission.

To correct the experimental M_R spectra alone, it is sufficient to evaluate from the simulations the ratio at each value of M_R of the yield within the (experimental) range $45\text{--}135^\circ$ to the total yield. These ratios (denoted efficiencies) are shown in Figs. 6(g)–6(i). At the middle energy, the efficiency for mass-asymmetric fast quasifission is high, since the typical rotation angle places most quasifission events within the experimental angular coverage. Dividing the observed counts for each mass split by the efficiency determined through the simulation gives the total yield for each mass split. As would be expected, the efficiencies for each reaction showed a similar trend with E/V_B .

3. Fitting mass-ratio spectra

With the efficiency-corrected mass-ratio yields determined at each bombarding energy for each reaction, the ratio of mass-asymmetric to mass-symmetric fission events can be investigated quantitatively for the first time. Figure 7 shows representative efficiency-corrected mass-ratio spectra (blue circles). These range from predominantly mass-asymmetric

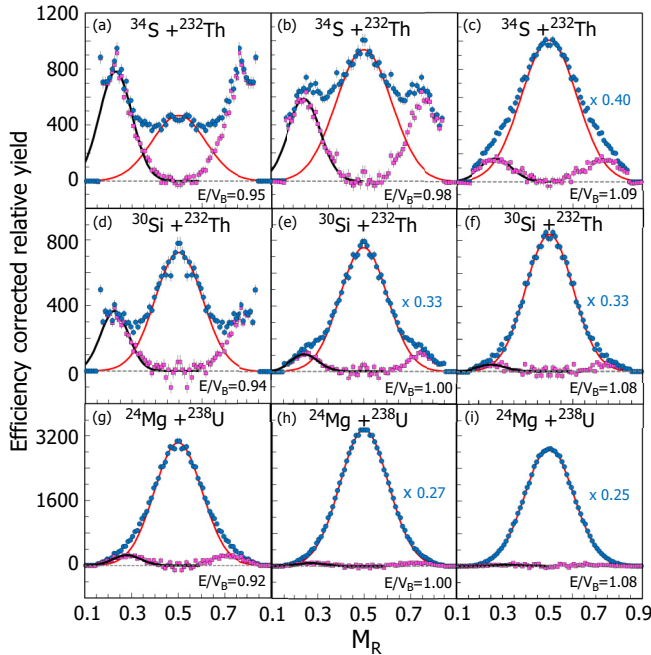


FIG. 7. Representative mass-ratio spectra (blue circles) for the reactions and energies indicated, corrected for detection efficiency as determined in Fig. 6. With the goal of extracting relative yields of the symmetric-peaked and mass-asymmetric components, the mass-symmetric yield was matched to a Gaussian (red curve). Subtracting this gives the residuals (magenta squares). These in turn were fitted with Gaussians (black curves). The ratio of asymmetric to symmetric fission yields were then determined for all measurements (see text).

fission in Fig. 7(a) for the low energy $^{34}\text{S} + ^{232}\text{Th}$ measurement to almost exclusively mass-symmetric for the high energy $^{24}\text{Mg} + ^{238}\text{U}$ measurement, shown in Fig. 7(i). The high energy data for each reaction suggest that the mass-symmetric component can be well represented by a Gaussian, and indicate the appropriate width for this component. Since the mass-

symmetric component corresponds to fissionlike events with the longest time scales, it is closer to equilibrium than the mass-asymmetric events, so the assumption of a Gaussian distribution for this component seems justifiable.

For the reactions forming ^{266}Sg , an average symmetric component mass-ratio width σ_{MR} of 0.117 was needed, ranging from 0.115 at the lowest energies, to a highest value of 0.119. For ^{262}Rf , a smaller average σ_{MR} was needed, typically 0.103, with a small variation of ± 0.001 . The mass-symmetric Gaussians (shown by the red lines) were fitted to the experimental yield around mass symmetry, and the residuals are shown by the magenta square points.

The residuals closely match a Gaussian shape (black lines). Gaussian fits were used to estimate the yield of mass-asymmetric quasifission in the region at large asymmetry, which is masked by the elastic scattering events. The total mass-asymmetric yield was taken from the Gaussian yield from the largest mass asymmetries up to the peak, and from the sum of the residuals from the peak to mass symmetry. If it were to be shown that the asymmetric component should have a contribution reaching to mass symmetry, this would simply shift the asymmetric yield upwards by a similar small fraction at each energy, and would not have a significant effect on the final conclusions. This procedure allowed the ratio of mass-asymmetric to mass-symmetric events to be evaluated for all reactions and energies, integrated over all center-of-mass angles.

4. Energy dependence of mass-asymmetric to mass-symmetric yields

First the experimental results and analysis for the $^{34}\text{S} + ^{232}\text{Th}$ reaction will be discussed fully, followed by the results and conclusions from the other reactions.

Figure 8(a) shows the beam energy dependence of the ratio of the mass-asymmetric to symmetric fission yields. The yellow points show the ratios before correcting for the mass-asymmetry dependent efficiency (see Fig. 6), and the red points the ratios after correction. As expected, where the

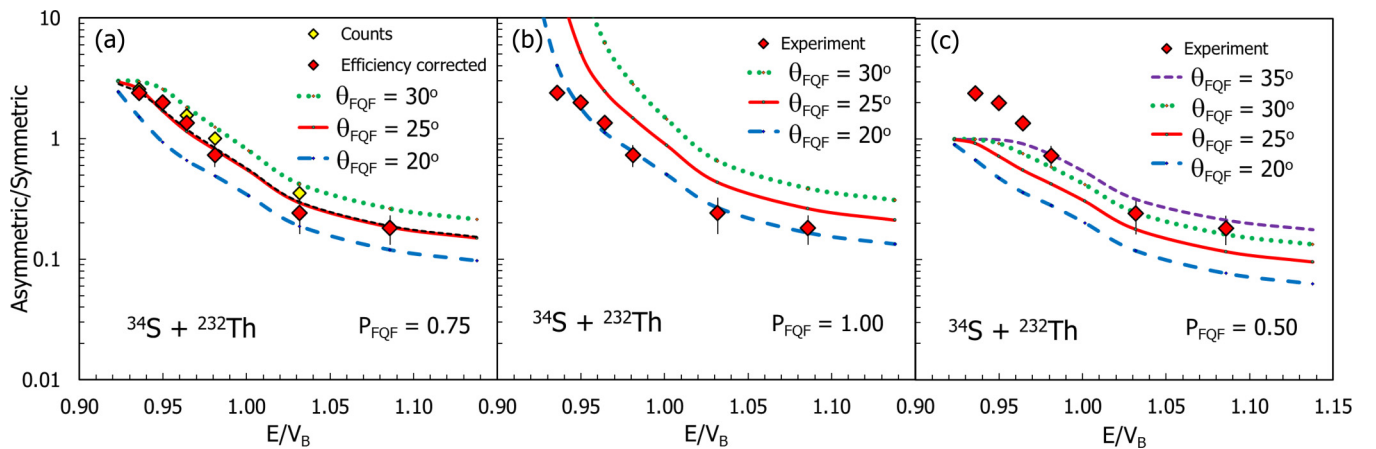


FIG. 8. Ratio of the mass-asymmetric to symmetric-peaked fission yields for the $^{34}\text{S} + ^{232}\text{Th}$ reaction as a function of E/V_B . Experimental results with efficiency correction are shown by the red diamonds, and without by yellow diamonds in panel (a). To illustrate the sensitivity of the energy dependence to model parameters, panels (a)–(c) show calculations for different values of the assumed probability of fast mass-asymmetric quasifission (P_{FQF}) in axial (tip) collisions. In each panel calculations for a range of angles θ_{FQF} dividing axial from equatorial collisions are shown. Chi-squared analysis gave the best fitting model parameters (see text).

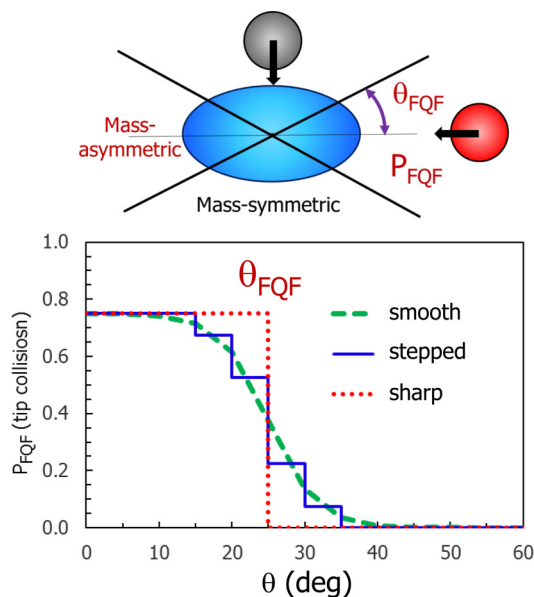


FIG. 9. At the top is a sketch of the simple ansatz used to model the ratio between fast mass-asymmetric quasifission and symmetric-peaked fission. Axial collisions up to a limiting angle θ_{FQF} are assumed to result in fast quasifission with probability P_{FQF} . Other collisions are taken to result in symmetric-peaked fissionlike events. The schematic illustration below shows P_{FQF} as a function of θ , with the sharp cutoff of P_{FQF} shown by the red dotted line. A more realistic smooth cutoff (green dashed line) can be approximated by a stepped function, but use of this makes little change to the results (see text).

efficiency for mass asymmetric events is high, around V_B [see Fig. 6(h)], the ratio falls after efficiency correction.

The asymmetric to symmetric yield ratio drops by a factor of 10 as the beam energy increases through the capture barrier energy. Qualitatively, this was recognized [43,47,49] to be due to the predominance of deformation-aligned (elongated) capture events at sub-barrier energies, resulting in fast mass-asymmetric quasifission. This contrasts with the predominance of compact equatorial collisions at energies well above barrier. These lead to longer sticking times (and also fusion), allowing greater mass equilibration resulting in fission with mass splits closer to symmetry. Having been able to determine the ratio of fast to slow events over the complete angular range for the first time, quantitative interpretation is now possible.

5. Fast quasifission ansatz

To make a quantitative prediction of the asymmetric to symmetric yield ratio, we follow the approach described in Refs. [35,36,51], originally applied to fission angular anisotropies rather than fast/slow quasifission yield ratios. Figure 9 illustrates the concept. We assign the fast mass-asymmetric quasifission (FQF) component to axial collisions. These are defined as those collisions with angles up to a limiting angle θ_{FQF} between the line joining the projectile-target centers and the actinide nucleus deformation axis at the capture barrier radius. This is illustrated in the upper sketch. The value of θ_{FQF} will be determined by reproducing the experimental data.

We also define a probability P_{FQF} that axial collisions lead to fast quasifission. Different options describing the variation of P_{FQF} with the angle between the centers of the projectile and target nuclei and the deformation axis are graphed below. In the simplest approach, the probability falls from P_{FQF} to zero at the critical angle θ_{FQF} , shown by the dotted red line. In reality, a smooth transition would be expected (green dashed line). The effect of this has been investigated by approximating it by a weighted sum of calculations with different values of θ_{FQF} (blue stepped line). The separate cross sections for the axial and equatorial components of the total capture cross section were determined using coupled-channel calculations of capture as described in Ref. [42], for different values of θ_{FQF} .

There is no guarantee that the quantities P_{FQF} and θ_{FQF} are independent of beam energy. However, relevant energies for heavy element formation reactions are close to the average barrier energy, and the fit to the experimental data encompasses an energy span $0.9 < E/V_B < 1.1$, so this concern may not be significant in this work.

6. Comparison with experiment

A comparison of the predicted energy dependence of the asymmetric to symmetric fission yields is shown in Fig. 8(b), for different values of θ_{FQF} , where P_{FQF} for axial collisions has been set to unity. In this case, at the lowest energies, the calculated ratio rises to very large values. This is because the change in capture barrier energy with angle is large compared with the energy smearing due to quantum tunneling [21].¹ The calculation for $\theta_{\text{FQF}} = 20^\circ$ gives quite a good representation of the data. Figure 8(c) shows similar calculations where $P_{\text{FQF}} = 0.5$ for all θ_{FQF} . Here all calculations by definition saturate at a ratio 1.0, which is not consistent with experiment. These comparisons illustrate the degree to which the data constrain the model parameters.

A chi-squared analysis over θ_{FQF} and P_{FQF} was performed, and the optimal values and uncertainties of each parameter were determined. The optimum P_{FQF} was 0.76, and θ_{FQF} was 25° . This is very close to the red curve shown in Fig. 8(a). The effect of applying a stepped variation of P_{FQF} with angle (similar to that illustrated in Fig. 9) is shown by the dotted black line. This overlies the red line resulting from the sharp cutoff assumption, showing that this smoothing would have a negligible effect on the analysis and conclusions.

7. Systematic behavior

The fitting procedure using the sharp-cutoff assumption was carried out for the three other reactions. The experimental asymmetric to symmetric fission yield ratios for these reactions, and representative calculations with $\theta_{\text{FQF}} = 20^\circ$, are shown in Fig. 10. The $^{28}\text{Si} + ^{238}\text{U}$ data, which extend to the lowest E/V_B , show saturation at the lowest energy, providing the tightest constraint on the fit parameters. Any

¹Similar calculations carried out for an alpha-particle projectile, where the width of the capture barrier distribution is similar to the single barrier tunneling width [21], would show a much weaker variation with energy.

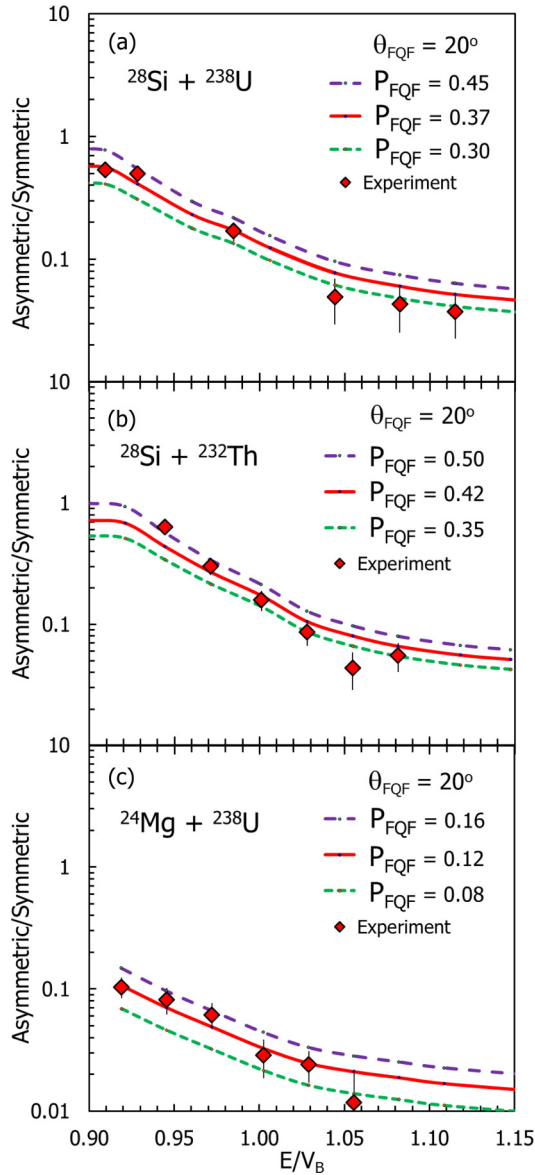


FIG. 10. As in Fig. 8, for the other three reactions studied. Here a fixed value of $\theta_{\text{FQF}} = 20^\circ$ is used, and calculations for various values of P_{FQF} are shown. As for the $^{34}\text{S} + ^{232}\text{Th}$ data, a chi-squared fit gave best values of θ_{FQF} and P_{FQF} .

future measurements should be taken as low in energy as possible, since even a 10% uncertainty in the ratio measured at or below $E/V_B = 0.9$ will provide an important constraint.

The best-fitting values of θ_{FQF} and P_{FQF} , with experimental uncertainties, are shown in Figs. 11(a) and 11(b) respectively by the red circles (^{232}Th) and orange triangles (^{238}U), plotted as a function of the projectile atomic number Z_P . P_{FQF} shows a strong increase with Z_P . This can be parametrized with a Fermi function centered at $Z_P = 14$, as shown by the magenta line. With the target atomic number only changing by 2 from Th to U, any dependence on this variable cannot be established, except to say it is weaker than the dependence on Z_P . This is reasonable, in light of the results of the global survey of quasifission presented in Ref. [5], where the charge product

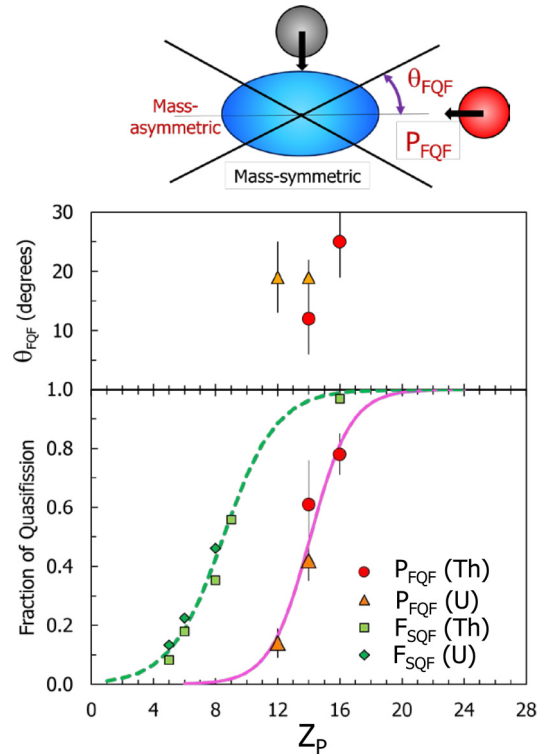


FIG. 11. Results of application of the fast quasifission ansatz (illustrated again at the top) to the four reactions, as a function of projectile atomic number Z_P . Panel (a) shows the best-fitting values of θ_{FQF} . Experimental uncertainties (from the chi-squared analysis) prevent definitive determination of the dependence on Z_P , though the data are consistent with an increasing trend, which might be expected. Panel (b) shows the dependence of P_{FQF} on Z_P (circles and triangles for Th and U respectively). A rapid rise is seen, as expected even from the raw M_R spectra. Also shown are the probabilities for slow quasifission estimated from the angular distributions of the symmetric-peaked fission (see Sec. III C).

in the entrance channel is globally the strongest driver of quasifission characteristics.

The experimental uncertainties in θ_{FQF} , as shown in Fig. 11(b), do not allow an unambiguous dependence on Z_P to be established, although an increasing trend with Z_P might be expected, and the data are consistent with this. More extensive data for projectiles heavier than S, measured over an even wider range of angles to reduce sensitivity to extrapolation of the systematics to reactions planned to be used to synthesize the next superheavy elements. However, where the probabilities for symmetric mass splits become small, the decomposition of the mass distribution becomes problematic, since the tails of the fast mass-asymmetric quasifission may contribute significantly even in the region close to mass symmetry [52]. In this case measurements of mass-angular distributions over a wide angular range, as well as TKE distributions (also extended to a wider angular range), may allow the different components in the mass-symmetric events to be decomposed.

Having made a quantitative analysis of fast quasifission probabilities in axial collisions, it is natural to turn to char-

acterization of the mass-symmetric events in axial collisions (those that survive the fast quasifission process) to investigate the competition between quasifission and fusion-fission components as a function of the projectile charge.

C. Angular distribution of mass-symmetric fission events

The presence of a quasifission component in fission centered on mass symmetry has been investigated through measurement and analysis of fission fragment angular distributions [53–55]. These are usually characterized by the ratio of the (extrapolated) yield at 0° or 180° to that at 90° in the c.m. frame, known as the angular anisotropy A . The saddle-point transition state model (TSM) has been widely used to predict fusion-fission angular distributions and anisotropies [56,57]. For reactions such as $^{16}\text{O} + ^{208}\text{Pb}$, where quasifission is not expected, the saddle-point TSM was able to describe quite well the measured fission anisotropies [58,59].

In one of the first studies of quasifission, experimental (symmetric) fission angular distributions showed increased anisotropies compared with TSM predictions in capture reactions of a range of heavy projectiles with ^{208}Pb [54]. Deviations increased with increasing Z_P , attributed to an increasing contribution from quasifission.

The relationship between quasifission identified through angular anisotropies and other quasifission observables (focusing on reactions forming Cm isotopes) has been discussed in Ref. [41]. As shown there, an angular range of 45° – 135° , as in the present work, is not sufficient to provide a good measure of the angular anisotropy. Thus to investigate the nature of the mass-symmetric fission events through anisotropies, experimental data were sought in the literature.

1. Experimental anisotropies for reactions with Th,U targets

In reactions with actinide target nuclei, angular distributions for fission centered on mass symmetry have been measured for projectile nuclei from Li to S, bombarding targets including Th and U [60]. In analogy with the interpretation for reactions on ^{208}Pb , it was proposed [35,36] that large anisotropies at sub-barrier energies (exceeding TSM predictions for fusion fission) are a signature of a slow quasifission process, which retains a “memory” of the deformation-aligned configuration, despite achieving an essentially symmetric peaked mass distribution. This results in forward-backward peaked angular distributions with large anisotropies A , in contrast with almost isotropic TSM predictions (small A) for fusion fission at sub-barrier energies.

An experimental difficulty is that fission events also arise following transfer reactions: at sub-barrier energies, the transfer yield can far exceed the yield of fission following capture [61]. However, measurement of fragment velocities (for example using a pulsed beam) allows separation by the v_{\parallel} and v_{\perp} method [36] which has been shown to be effective for projectiles as light as ^{12}C [51].

Experimental measurements of A have been selected from the literature [16,36,51,62–66] for reactions of projectiles from B to S, bombarding targets of ^{232}Th and ^{238}U . Selection was based on consistency between measurements by different authors, the effectiveness of the method of separation of transfer-

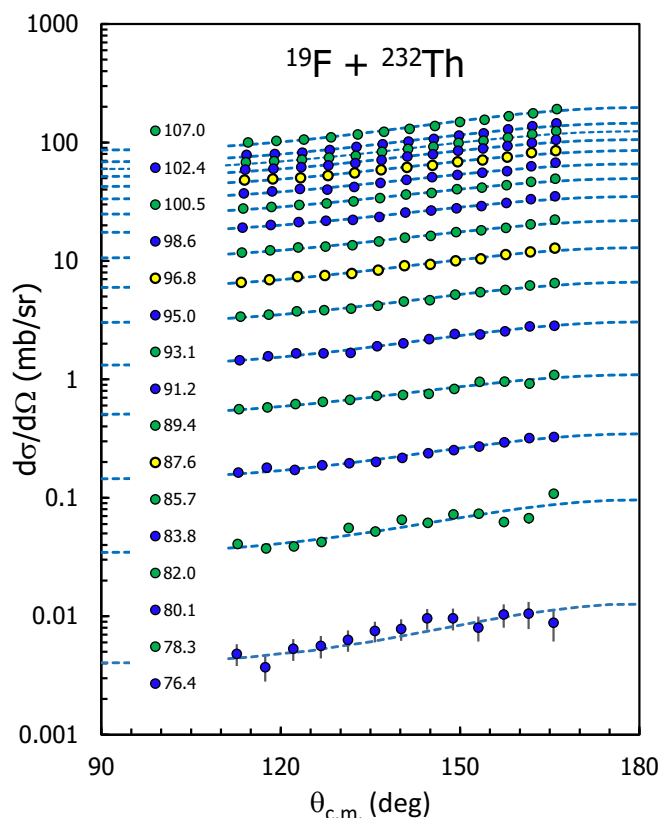


FIG. 12. Measured angular distributions from this work, for FMT fission in the $^{19}\text{F} + ^{232}\text{Th}$ reaction, at the indicated c.m. energies. Fits to the distributions using the transition state model formalism are shown by the dashed lines, where K_0 was a free parameter. The different colored symbols serve to correlate the data with the c.m. energies. The anisotropies were determined from the ratio of the value of the fit at 180° to that at 90° .

induced fission (and its likely influence on the anisotropies), and the consistent variation of A as a function of beam energy within a given experiment.

To complement the results from the literature, measurements from the ANU for the reactions $^{12}\text{C} + ^{238}\text{U}$ and $^{19}\text{F} + ^{232}\text{Th}$ have been added. These were measured and analyzed using the experimental methods and techniques described in detail for the similar reactions $^{16}\text{O} + ^{238}\text{U}$ and $^{12}\text{C} + ^{232}\text{Th}$ in Refs. [36] and [51] respectively.

In all these measurements, it is necessary to extrapolate the data to 0° or 180° in order to estimate an anisotropy. This is generally achieved using TSM fits, using a single value of K_0 , which as discussed later may well not be appropriate. However, since the interpretation of the extracted A values described below is as yet qualitative, and there is currently no predictive model of slow quasifission angular distributions, this procedure is also used for the new data presented here.

The measured angular distributions for FMT fission for the $^{19}\text{F} + ^{232}\text{Th}$ reaction are shown in Fig. 12. The blue dashed lines show the TSM fits used to extrapolate to 180° and 90° in order to determine anisotropies. The FMT fission cross sections determined from these TSM fits are shown in Fig. 13 as a function of E/V_B . Also shown are estimated transfer-fission

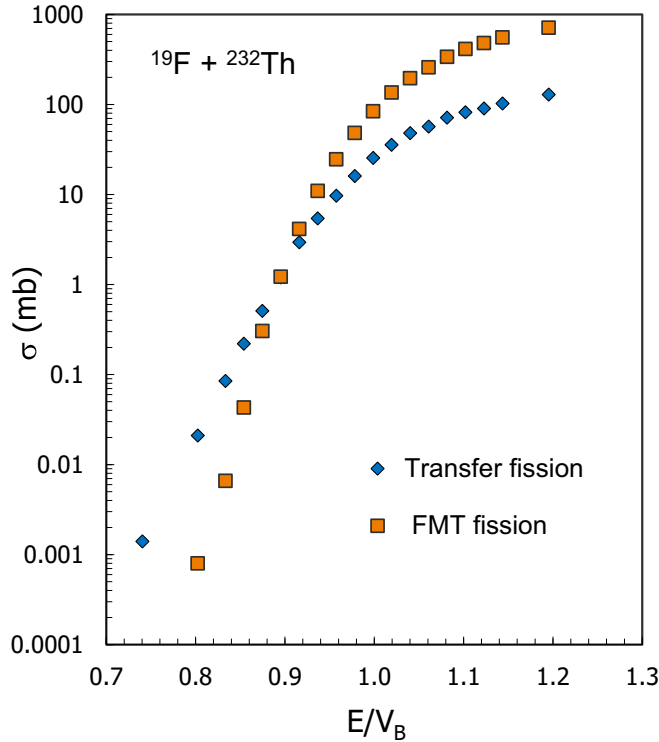


FIG. 13. Cross sections for FMT fission (orange points) for the $^{19}\text{F} + ^{232}\text{Th}$ reaction, as a function of E/V_B . The average barrier energy V_B was determined to be 89.5 MeV. Also shown are estimated cross sections for fission events where most of the mass of the projectile was not absorbed, most likely following transfer reactions. The cross section of transfer fission exceeds that of FMT fission at around $E/V_B = 0.90$, and at $E/V_B = 0.80$, it is difficult to identify reliably the FMT fission events.

cross sections. It is clear that the latter can be dominant at energies well below the average capture barrier. The increasing fraction of transfer-induced fission provides a limitation on how low in energy FMT fission angular distributions can be reliably determined [61].

2. Systematic behavior of anisotropies

The angular anisotropies for all the reactions considered are shown in Fig. 14. For the lighter projectiles including ^{19}F , the fission mass distributions are peaked at mass symmetry, and the anisotropies are those for all FMT fission events. For the $^{32}\text{S} + ^{232}\text{Th}$ reaction, as described in Ref. [16], the anisotropies are those only for mass splits around symmetry, namely $0.4 < M_R < 0.6$, thus excluding most of the fast mass-asymmetric quasifission events. TSM calculations for many of the reactions are shown by the lines, whose colors match those of the experimental data points for each reaction.

The energy dependence of the experimental values of A compared with the TSM calculations is qualitatively similar for all reactions with the heavier projectile nuclei. At the lowest energies ($E/V_B \sim 0.95$) the measurements are significantly higher than the TSM prediction, they then fall to a minimum at $1.02 < E/V_B < 1.04$ (though still well above the TSM calculation), then rise again. As in the analysis of the ratio of

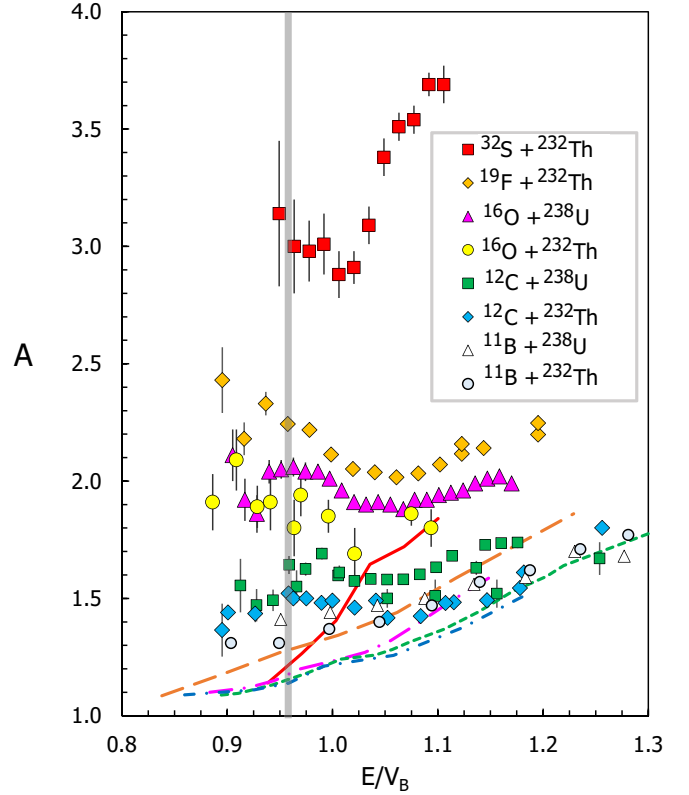


FIG. 14. Symmetric-peaked fission angular anisotropies A as a function of E/V_B for the indicated reactions. The curves represent TSM calculations of fusion-fission anisotropies. They are color coded to the reaction symbol.

mass-asymmetric to mass-symmetric yields, this behavior has been associated with the transition from predominantly axial collisions at sub-barrier energies to predominantly equatorial collisions at high energies [36,65,67].

A key feature of the systematics in Fig. 14 is the strong increase in the measured anisotropies at sub-barrier energies as a function of projectile charge Z_P . At $E/V_B = 0.96$, for the lightest projectile ^{11}B , $A \sim 1.3$ – 1.4 . This increases to ~ 1.6 for ^{12}C , 1.9 for ^{16}O , 2.2 for ^{19}F , and finally ~ 3.0 for ^{32}S . In contrast, TSM predictions lie in the range 1.15 – 1.30 . It would seem reasonable to link these greatly increased anisotropies to an increasing contribution from quasifission. While it is currently not possible to accurately predict the slow quasifission anisotropy, some limits can be set on the probability of slow quasifission.

3. Expectations for quasifission anisotropies

Before the measurements were made [16] showing very large anisotropies for $^{32}\text{S} + ^{232}\text{Th}$, in the original interpretation of the $^{16}\text{O} + ^{238}\text{U}$ results it had been assumed that the axial (tip) collisions at sub-barrier energies resulted solely from quasifission (i.e. $P_{\text{SQF}} = 1$), thus defining A_{SQF} . Subsequent measurements of evaporation residues at sub-barrier energies were interpreted [68,69] as showing that $P_{\text{SQF}} = 0$. A value between these extremes (such as 0.5) could explain both the large anisotropies and the

observation of ERs. For a value of P_{SQF} around 0.5, the slow quasifission anisotropies would have to be considerably larger than the experimental sub-barrier anisotropies for $^{16}\text{O} + ^{238}\text{U}$.

The more recent $^{32}\text{S} + ^{232}\text{Th}$ measurements show that the quasifission anisotropy can be very large, even at sub-barrier energies where the orbital angular momenta are rather low. But could this value be appropriate for reactions with lighter projectiles? To address this consider the simplest expression for the anisotropy, namely $A = 1 + \langle J^2 \rangle / 4K_0^2$, where $\langle J^2 \rangle$ is the mean square angular momentum of the nuclei undergoing fission, and K_0^2 is the variance of the projections of J onto the fission axis.

For the same above-barrier value of E/V_B , and for the same channel couplings, the value of $\langle J^2 \rangle$ should scale with the projectile reduced mass. For fusion fission, the equilibrium value of K_0^2 would be expected to take similar values for each reaction, only differing due to changes in temperature at the saddle point (excitation energy). Thus the fusion-fission anisotropies (TSM anisotropies) should fall significantly for lighter projectiles. This is reflected in the calculated TSM values shown in Fig. 14.

However, we are here considering quasifission, where the value of K_0^2 is far below its equilibrium value. It was pointed out in Ref. [70] that the tilting relaxation time, most closely related to the K degree of freedom, is inversely proportional to the square of the rotational frequency. To first order this dependence cancels the $\langle J^2 \rangle$ term in the expression for the anisotropy. Therefore it may not be unreasonable to expect that the quasifission anisotropy at similar E/V_B may be similar for the different reactions.

4. Estimating the slow quasifission component

Defining the anisotropy for slow mass-symmetric quasifission to be that measured for $^{32}\text{S} + ^{232}\text{Th}$, all the ingredients are in place to estimate the fraction of the symmetric-peaked fission events that result from slow quasifission. The measured anisotropy $A(Z_P)$ for a given projectile (identified by Z_P) is the weighted sum of the fusion-fission and quasifission anisotropies:

$$A(Z_P) = F_{\text{SQF}}(Z_P)A_{\text{SQF}}(Z_P) + [1 - F_{\text{SQF}}(Z_P)]A_{\text{TSM}}(Z_P), \quad (2)$$

where the fraction of slow quasifission for each reaction is $F_{\text{SQF}}(Z_P)$, and the anisotropy for fusion fission $A_{\text{TSM}}(Z_P)$ is taken to be that calculated with the transition state model. The desired $F_{\text{SQF}}(Z_P)$ is then given by

$$F_{\text{SQF}}(Z_P) = \frac{A(Z_P) - A_{\text{TSM}}(Z_P)}{[A_{\text{SQF}}(Z_P) - A_{\text{TSM}}(Z_P)]}. \quad (3)$$

The main assumption lies in the values of $A_{\text{SQF}}(Z_P)$, taken to be 3.2 for all reactions. There is some uncertainty in the values of A_{TSM} , but this is likely to be small in comparison with the uncertainty in $A_{\text{SQF}}(Z_P)$.

The values of F_{SQF} extracted using Eq. (3) are shown in Fig. 11(b) by the green symbols. These show a smooth increase with projectile charge Z_P . The behavior is similar to that of the fast quasifission, displaced to lower Z_P , with

the SQF transition being centered at $Z_P = 8$ instead of 14. Uncertainties are not plotted, as they arise mainly from the assumptions regarding $A_{\text{SQF}}(Z_P)$ and A_{TSM} , rather than experimental uncertainties. It must be emphasized that the resemblance to the behavior of P_{FQF} with Z_P should not be taken as evidence that the assumptions made are correct. The effect of changing the assumed value or Z dependence of $A_{\text{SQF}}(Z_P)$ and $A_{\text{TSM}}(Z_P)$ can readily be found through Eq. (3).

The qualitative results do provide encouragement to extend experimental measurements of angular anisotropies for Th and U targets to projectiles between F and S, and to extend measurements for all projectiles to a larger range of actinide target nuclei.

A complementary approach to determine the relative yields of fusion-fission and quasifission has been proposed by Itkis *et al.* [44], through measurement of structure in total kinetic energy (TKE) distributions as a function of fission mass split. This is complicated by bimodal fusion fission, also having different TKE distributions [44].

For the low energy reaction $^{24}\text{Mg} + ^{248}\text{Cm}$, the measured symmetric fission TKE distribution (Fig. 7 of Ref. [44]) shows a low energy and a high energy component. The latter was proposed as resulting from ‘‘symmetric compact fission’’—i.e., fusion fission. The present work would suggest that the low energy component might be identified with slow quasifission rather than another fusion-fission mode. With this assumption, the fraction of slow quasifission can be determined from the decomposition in Ref. [44] to be around 0.75. This is in reasonable agreement with the trends of our qualitative analysis of angular anisotropies presented in Fig. 11(b), suggesting that this interpretation is not unreasonable.

In future, combining mass, TKE, and angular distributions might offer the most promising approach to decomposing fission yields centered on mass symmetry into both slow quasifission and different fusion-fission modes. Such measurements would be challenging, due to the requirements for high statistics, and the low capture cross sections at sub-barrier energies.

IV. DISCUSSION AND CONCLUSIONS

Following the first firm experimental evidence for quasifission [71], the exhaustive pioneering work at GSI [1,2] in the 1980s measuring mass-angle distributions for reactions with ^{238}U first defined key characteristics of the quasifission process. In particular, systematics of mass distributions, total kinetic energies, and quasifission time scales were established. This set the scene for subsequent investigations of quasifission dynamics, notably through investigation of time scales by different techniques [3,72–77]. The mass-angle distribution method, developed at GSI, has arguably proven to be the best-suited technique to determine the average reaction time scales up to 10 zs, or half of a full revolution of the system.

A major advance since the GSI work has been the development of an understanding of the crucial role played by the static deformation of actinide nuclei. Beyond its general importance in capture [21–28], in heavy element synthesis reactions it is also found to be crucial in determining the subsequent shape evolution, resulting either in a compact compound nucleus

(fusion) or in quasifission [16,35–39,42,43,45,47,78,79]. Fundamentally this is a result of the initial shape at capture ranging from elongated to compact, depending on whether the lighter nucleus makes contact with the tip or equator of the prolate deformed actinide nuclei. This has been described in more detail in Sec. IC2, and in the above references.

The current work explores quantitatively the competition between fusion and quasifission in sub-barrier reactions with actinide target nuclei. It has been argued [16] that in order to form a compact compound nucleus (i.e., to fuse), the system has to survive *two* faster competing quasifission processes. In the current work, their distinct characteristics, which suggest bifurcations in trajectories and associated reaction times, are investigated systematically to extract probabilities of each process.

In order of reaction time, the first of these processes is the mass-asymmetric quasifission whose peaked angular distributions demonstrate directly its fast time scale. This we call here fast quasifission (FQF). As has been shown, this is strongly correlated with deformation alignment. Model comparisons with experimental MAD show that this occurs on time scales of a few zeptoseconds [39,42], and resulting in a very asymmetric mass split. It appears that the mechanism responsible for these characteristics is related to shell structure in the potential energy surface of the elongated system before scission, perhaps associated with a doubly magic ^{208}Pb fragment. However, not all characteristics are consistent with this, and there may also be a dynamical aspect to this process.

The second process, corresponding to quasifission with a mass distribution peaked near mass symmetry, we call slow quasifission (SQF). In the measurements presented here the SQF mass distribution is quite distinct from the mass-asymmetric FQF distribution, since the former is peaked at mass symmetry. Several characteristics of the SQF events are not consistent with expectations for fusion fission, as detailed below.

For the measurements presented here, the clearest characteristics are (i) the mass widths, which are larger than expected for fusion fission, and (ii) the angular distributions, which are more anisotropic (closer to $1/\sin\theta$). Because the compound nuclei formed are fissile, rather isotropic fusion-fission angular distributions in $d\sigma/d\Omega$ are expected within the saddle-point TSM picture. This comes about because of the compact nuclear shape at the saddle point, resulting in rather little energy being required to tilt the fission axis from the normal to the angular momentum vector, leading to a wide distribution of K . This results in rather isotropic calculated angular distributions. A narrowing of the K distribution during the descent from saddle to scission is expected [80], but this would not be sufficient to explain the experimental energy dependence. Further quantitative experimental and theoretical investigation is required.

A third clear characteristic of quasifission is a correlation of the distribution of mass split with angle, signaling that some component of the quasifission time distribution is shorter than the time for half a rotation of the composite system. However, this is not a necessary condition for the presence of quasifission, if its time scale is sufficiently long. There is evidence of mass-angle correlations in the present data, but higher statistics

and a wider angular range would be valuable to quantify this.

A fourth characteristic has been proposed which may distinguish slow quasifission from (some) fusion-fission modes, namely the total kinetic energy. Here again more detailed experimental studies will be important, ideally correlating the TKE, angle and mass distributions to try to obtain a consistent picture from all these observables.

A proposal [81] was made to explain unexpectedly large fission anisotropies through the assumption that fusion fission can occur equilibrated in all degrees of freedom except K . This picture took the view (extrapolating from a model for deep-inelastic reactions) that the K -equilibration time can be slower than the fusion-fission time scale, therefore resulting in large anisotropies without needing to propose a fission process faster than fusion fission. However, it was later argued [57] that K -equilibration times for compact compound nucleus shapes should be very fast, throwing doubt on the basis for this proposal except where the fission barrier is lower than the nuclear temperature [57].

In the present reactions, measured at near-barrier energies, the fission barrier height is larger than the temperature. Furthermore, the mass widths and mass-angle correlations indicate that the slow quasifission must be faster than fusion fission. Being faster, slow quasifission must suppress the fusion yield [67], just like fast quasifission. Some insights into the nature of SQF can be taken from Langevin transport model calculations. Here fission occurs from systems that have never reached the equilibrium pocket, but have passed inside the saddle point. This has been called “deep quasifission” [82]. For consistency, we will use the terms fast quasifission and slow quasifission to distinguish processes that differ in their empirical (observed) characteristics, in particular the time scale measured by the mass-angle correlation and/or inferred from the amount of mass equilibration.

The preliminary nature of the extracted dependence of the slow quasifission probability on the projectile charge makes it premature to discuss in detail the reasons for the dependence that is observed. However, it is likely that the Businaro-Gallone mass asymmetry, which has been discussed extensively in the literature (e.g., Refs. [48,67], and references therein), is playing a significant role. The relationship of the entrance channel mass asymmetry and the Businaro-Gallone asymmetry determines whether mass tends to flow from the projectilelike nucleus, resulting in its absorption (fusion), or flows to the projectilelike nucleus. This will be the subject of a future paper.

Here we concentrate on the effects of both fast and slow quasifission in determining P_{CN} in sub-barrier reactions with prolate deformed actinide target nuclei. With the understanding that these quasifission processes are sequential, rather than simultaneous, P_{CN} can be written as the product of the probability of surviving each process, in terms of the empirical probabilities P_{FQF} and F_{SQF} determined from experiment:

$$P_{\text{CN}} = (1 - P_{\text{FQF}})(1 - F_{\text{SQF}}). \quad (4)$$

For reactions with projectiles heavier than $Z = 16$, the current results indicate that both these probabilities are small. Thus the probability of forming superheavy elements at below barrier energies does not appear to be favorable. However, the smaller

values of P_{CN} at sub-barrier energies could be offset by a much higher value of compound nucleus fission survival probability. It is necessary to try to determine how each of these quasifission probabilities changes with entrance channel conditions (particularly charge product), both experimentally (in particular through measurements for projectiles with higher Z_p) and with the help of theoretical calculations that are able to describe the current and new observations.

With further work, it may be possible to tie together more extensive future measurements of quasifission and evaporation residue cross sections to develop the ultimate goal of a detailed

and quantitative predictive capacity for all superheavy element formation reactions.

ACKNOWLEDGMENTS

The authors acknowledge support from ARC Grants No. FL110100098, No. DP130101569, No. FT120100760, No. DE140100784, No. DP140101337, No. DP160101254, and No. DP170102318, and support by the Federal Government NCRIS program for operations of the ANU Heavy Ion Accelerator Facility.

-
- [1] J. Töke, B. Bock, G. X. Dai, A. Gobbi, S. Gralla, K. D. Hildenbrand, J. Kuzminski, W. F. J. Müller, A. Olmi, and H. Stelzer, *Nucl. Phys. A* **440**, 327 (1985).
- [2] W. Q. Shen, J. Albinski, A. Gobbi, S. Gralla, K. D. Hildenbrand, N. Herrmann, J. Kuzminski, W. F. J. Müller, H. Stelzer, J. Töke, B. B. Back, S. Bjørnholm, and S. P. Sørensen, *Phys. Rev. C* **36**, 115 (1987).
- [3] D. J. Hinde, D. Hilscher, H. Rossner, B. Gebauer, M. Lehmann, and M. Wilpert, *Phys. Rev. C* **45**, 1229 (1992).
- [4] R. du Rietz, D. J. Hinde, M. Dasgupta, R. G. Thomas, L. R. Gasques, M. Evers, N. Lobanov, and A. Wakhle, *Phys. Rev. Lett.* **106**, 052701 (2011).
- [5] R. du Rietz, E. Williams, D. J. Hinde, M. Dasgupta, M. Evers, C. J. Lin, D. H. Luong, C. Simenel, and A. Wakhle, *Phys. Rev. C* **88**, 054618 (2013).
- [6] Y. T. Oganessian, *Lect. Notes Phys.* **33**, 221 (1975).
- [7] P. Armbruster, *Annu. Rev. Nucl. Part. Sci.* **50**, 411 (2000).
- [8] S. Hofmann and G. Münzenberg, *Rev. Mod. Phys.* **72**, 733 (2000).
- [9] S. Hofmann, F. P. Heßberger, D. Ackermann, G. Münzenberg, S. Antalic, P. Cagarda, B. Kindler, J. Kojouharova, M. Leino, B. Lommel, R. Mann, A. G. Popeko, S. Reshitko, S. Šaro, J. Uusitalo, and A. V. Yeremin, *Eur. Phys. J. A* **14**, 147 (2002).
- [10] V. I. Zagrebaev, A. V. Karpov, and W. Greiner, *Phys. Rev. C* **85**, 014608 (2012).
- [11] Yu. Ts. Oganessian, V. K. Utyonkov, Y. V. Lobanov, F. S. Abdullin, A. N. Polyakov, R. N. Sagaidak, I. V. Shirokovsky, Y. S. Tsyganov, A. A. Voinov, G. G. Gulbekian, S. L. Bogomolov, B. N. Gikal, A. N. Mezentsev, S. Iliev, V. G. Subbotin, A. M. Sukhov, K. Subotic, V. I. Zagrebaev, G. K. Vostokin, M. G. Itkis *et al.*, *Phys. Rev. C* **74**, 044602 (2006).
- [12] Yu. Ts. Oganessian, F. S. Abdullin, P. D. Bailey, D. E. Benker, M. E. Bennett, S. N. Dmitriev, J. G. Ezold, J. H. Hamilton, R. A. Henderson, M. G. Itkis, Y. V. Lobanov, A. N. Mezentsev, K. J. Moody, S. L. Nelson, A. N. Polyakov, C. E. Porter, A. V. Ramayya, F. D. Riley, J. B. Roberto, M. A. Ryabinin *et al.*, *Phys. Rev. Lett.* **104**, 142502 (2010).
- [13] Y. T. Oganessian, F. S. Abdullin, C. Alexander, J. Binder, R. A. Boll, S. N. Dmitriev, J. Ezold, K. Felker, J. M. Gostic, R. K. Grzywacz, J. H. Hamilton, R. A. Henderson, M. G. Itkis, K. Miernik, D. Miller, K. J. Moody, A. N. Polyakov, A. V. Ramayya, J. B. Roberto, M. A. Ryabinin *et al.*, *Phys. Rev. Lett.* **109**, 162501 (2012).
- [14] J. Khuyagbaatar, A. Yakushev, C. E. Düllmann, D. Ackermann, L.-L. Andersson, M. Asai, M. Block, R. A. Boll, H. Brand, D. M. Cox, M. Dasgupta, X. Derckx, A. Di Nitto, K. Eberhardt, J. Even, M. Evers, C. Fahlander, U. Forsberg, J. M. Gates, N. Gharibyan *et al.*, *Phys. Rev. Lett.* **112**, 172501 (2014).
- [15] Y. Oganessian and V. Utyonkov, *Nucl. Phys. A* **944**, 62 (2015), Special Issue on Superheavy Elements .
- [16] D. J. Hinde, R. du Rietz, M. Dasgupta, R. G. Thomas, and L. R. Gasques, *Phys. Rev. Lett.* **101**, 092701 (2008).
- [17] C. Simenel, D. J. Hinde, R. du Rietz, M. Dasgupta, M. Evers, C. J. Lin, D. H. Luong, and A. Wakhle, *Phys. Lett. B* **710**, 607 (2012).
- [18] A. Săndulescu, R. Gupta, W. Scheid, and W. Greiner, *Phys. Lett. B* **60**, 225 (1976).
- [19] Y. Aritomo, *Nucl. Phys. A* **780**, 222 (2006).
- [20] D. J. Hinde and M. Dasgupta, *Phys. Lett. B* **622**, 23 (2005).
- [21] M. Dasgupta, D. J. Hinde, N. Rowley, and A. M. Stefanini, *Annu. Rev. Nucl. Part. Sci.* **48**, 401 (1998).
- [22] R. G. Stokstad, Y. Eisen, S. Kaplanis, D. Pelte, U. Smilansky, and I. Tserruya, *Phys. Rev. Lett.* **41**, 465 (1978).
- [23] R. G. Stokstad, *Z. Phys. A* **295**, 269 (1980).
- [24] R. G. Stokstad and E. E. Gross, *Phys. Rev. C* **23**, 281 (1981).
- [25] W. Reisdorf, F. P. Heßberger, K. D. Hildenbrand, S. Hofmann, G. Münzenberg, K.-H. Schmidt, J. H. R. Schneider, W. F. W. Schneider, K. Sümmerer, G. Wirth, J. V. Kratz, and K. Schlitt, *Nucl. Phys. A* **438**, 212 (1985).
- [26] J. R. Leigh, M. Dasgupta, D. J. Hinde, J. C. Mein, C. R. Morton, R. C. Lemmon, J. P. Lestone, J. O. Newton, H. Timmers, J. X. Wei, and N. Rowley, *Phys. Rev. C* **52**, 3151 (1995).
- [27] C. R. Morton, A. C. Berriman, R. D. Butt, M. Dasgupta, D. J. Hinde, A. Godley, J. O. Newton, and K. Hagino, *Phys. Rev. C* **64**, 034604 (2001).
- [28] I. I. Gontchar, M. Dasgupta, D. J. Hinde, R. D. Butt, and A. Mukherjee, *Phys. Rev. C* **65**, 034610 (2002).
- [29] V. E. Oberacker, A. S. Umar, and C. Simenel, *Phys. Rev. C* **90**, 054605 (2014).
- [30] A. S. Umar, V. E. Oberacker, and C. Simenel, *Phys. Rev. C* **92**, 024621 (2015).
- [31] A. S. Umar, V. E. Oberacker, and C. Simenel, *Phys. Rev. C* **94**, 024605 (2016).
- [32] K. Sekizawa and K. Yabana, *Phys. Rev. C* **93**, 054616 (2016).
- [33] S. Raman, C. W. Nestor, Jr., and P. Tikkanen, *At. Data Nucl. Data Tables* **78**, 1 (2001).
- [34] A. Iwamoto, P. Möller, J. R. Nix, and H. Sagawa, *Nucl. Phys. A* **596**, 329 (1996).
- [35] D. J. Hinde, M. Dasgupta, J. R. Leigh, J. P. Lestone, J. C. Mein, C. R. Morton, J. O. Newton, and H. Timmers, *Phys. Rev. Lett.* **74**, 1295 (1995).

- [36] D. J. Hinde, M. Dasgupta, J. R. Leigh, J. C. Mein, C. R. Morton, J. O. Newton, and H. Timmers, *Phys. Rev. C* **53**, 1290 (1996).
- [37] S. Mitsuoka, H. Ikezoe, K. Nishio, and J. Lu, *Phys. Rev. C* **62**, 054603 (2000).
- [38] S. Mitsuoka, H. Ikezoe, K. Nishio, K. Satou, and J. Lu, *Phys. Rev. C* **65**, 054608 (2002).
- [39] A. Wakhle, C. Simenel, D. J. Hinde, M. Dasgupta, M. Evers, D. H. Luong, R. du Rietz, and E. Williams, *Phys. Rev. Lett.* **113**, 182502 (2014).
- [40] K. Nishio, H. Ikezoe, S. Hofmann, D. Ackermann, Y. Aritomo, V. F. Comas, C. E. Düllmann, S. Heinz, J. A. Heredia, F. P. Heßberger, K. Hirose, J. Khuyagbaatar, B. Kindler, I. Kojouharov, B. Lommel, M. Makii, R. Mann, S. Mitsuoka, I. Nishinaka, T. Ohtsuki *et al.*, *Nucl. Data Sheets* **119**, 299 (2014).
- [41] E. Williams, D. J. Hinde, M. Dasgupta, R. du Rietz, I. P. Carter, M. Evers, D. H. Luong, S. D. McNeil, D. C. Rafferty, K. Ramachandran, and A. Wakhle, *Phys. Rev. C* **88**, 034611 (2013).
- [42] E. Prasad, A. Wakhle, D. J. Hinde, E. Williams, M. Dasgupta, M. Evers, D. H. Luong, G. Mohanto, C. Simenel, and K. Vo-Phuoc, *Phys. Rev. C* **93**, 024607 (2016).
- [43] K. Nishio, H. Ikezoe, S. Mitsuoka, I. Nishinaka, Y. Nagame, Y. Watanabe, T. Ohtsuki, K. Hirose, and S. Hofmann, *Phys. Rev. C* **77**, 064607 (2008).
- [44] I. M. Itkis, E. M. Kozulin, M. G. Itkis, G. N. Knyazheva, A. A. Bogachev, E. V. Chernysheva, L. Krupa, Y. T. Oganessian, V. I. Zagrebaev, A. Y. Rusanov, F. Goennenwein, O. Dorvaux, L. Stuttgé, F. Hanappe, E. Vardaci, and E. de Goés Brennand, *Phys. Rev. C* **83**, 064613 (2011).
- [45] K. Nishio, H. Ikezoe, I. Nishinaka, S. Mitsuoka, K. Hirose, T. Ohtsuki, Y. Watanabe, Y. Aritomo, and S. Hofmann, *Phys. Rev. C* **82**, 044604 (2010).
- [46] K. Nishio, S. Mitsuoka, I. Nishinaka, H. Makii, Y. Wakabayashi, H. Ikezoe, K. Hirose, T. Ohtsuki, Y. Aritomo, and S. Hofmann, *Phys. Rev. C* **86**, 034608 (2012).
- [47] D. J. Hinde, R. G. Thomas, R. du Rietz, A. Diaz-Torres, M. Dasgupta, M. L. Brown, M. Evers, L. R. Gasques, R. Rafiei, and M. D. Rodriguez, *Phys. Rev. Lett.* **100**, 202701 (2008).
- [48] A. C. Berriman, D. J. Hinde, M. Dasgupta, C. R. Morton, R. D. Butt, and J. O. Newton, *Nature (London)* **413**, 144 (2001).
- [49] Y. Aritomo, K. Hagino, K. Nishio, and S. Chiba, *Phys. Rev. C* **85**, 044614 (2012).
- [50] E. V. Prokhorova, A. A. Bogachev, M. G. Itkis, I. M. Itkis, G. Knyazheva, N. A. Kondratiev, E. M. Kozulin, L. Krupa, Y. T. Oganessian, I. V. Pokrovsky, V. V. Pashkevich, and A. Y. Rusanov, *Nucl. Phys. A* **802**, 45 (2008).
- [51] J. C. Mein, D. J. Hinde, M. Dasgupta, J. R. Leigh, J. O. Newton, and H. Timmers, *Phys. Rev. C* **55**, R995(R) (1997).
- [52] E. M. Kozulin, G. N. Knyazheva, I. M. Itkis, M. G. Itkis, A. A. Bogachev, L. Krupa, T. A. Loktev, S. V. Smirnov, V. I. Zagrebaev, J. Äystö, W. H. Trzaska, V. A. Rubchenya, E. Vardaci, A. M. Stefanini, M. Cinausero, L. Corradi, E. Fioretto, P. Mason, G. F. Prete, R. Silvestri *et al.*, *Phys. Lett. B* **686**, 227 (2010).
- [53] B. B. Back, R. R. Betts, K. Cassidy, B. G. Glagola, J. E. Gindler, L. E. Glendenin, and B. D. Wilkins, *Phys. Rev. Lett.* **50**, 818 (1983).
- [54] B. B. Back, *Phys. Rev. C* **31**, 2104 (1985).
- [55] B. B. Back, R. R. Betts, J. E. Gindler, B. D. Wilkins, S. Saini, M. B. Tsang, C. K. Gelbke, W. G. Lynch, M. A. McMahan, and P. A. Baisden, *Phys. Rev. C* **32**, 195 (1985).
- [56] R. Vandenbosch and J. R. Huizenga, *Nuclear Fission* (Academic, New York, 1973).
- [57] D. J. Hinde, A. C. Berriman, M. Dasgupta, J. R. Leigh, J. C. Mein, C. R. Morton, and J. O. Newton, *Phys. Rev. C* **60**, 054602 (1999).
- [58] C. R. Morton, D. J. Hinde, J. R. Leigh, J. P. Lestone, M. Dasgupta, J. C. Mein, J. O. Newton, and H. Timmers, *Phys. Rev. C* **52**, 243 (1995).
- [59] D. J. Hinde, W. Pan, A. C. Berriman, R. D. Butt, M. Dasgupta, C. R. Morton, and J. O. Newton, *Phys. Rev. C* **62**, 024615 (2000).
- [60] S. Kailas, *Phys. Rep.* **284**, 381 (1997).
- [61] D. J. Hinde, M. Dasgupta, J. R. Leigh, D. G. Marinaro, and J. O. Newton, *Phys. Rev. Lett.* **81**, 4777 (1998).
- [62] Z. Liu, H. Zhang, J. Xu, Y. Qiao, X. Qian, and C. Lin, *Phys. Rev. C* **54**, 761 (1996).
- [63] J. P. Lestone, A. A. Sonzogno, M. P. Kelly, and D. Prindle, *Phys. Rev. C* **55**, R16(R) (1997).
- [64] J. P. Lestone, A. A. Sonzogno, M. P. Kelly, and R. Vandenbosch, *Phys. Rev. C* **56**, R2907(R) (1997).
- [65] J. P. Lestone, A. A. Sonzogno, M. P. Kelly, and R. Vandenbosch, *J. Phys. G: Nucl. Part. Phys.* **23**, 1349 (1997).
- [66] N. Majumdar, P. Bhattacharya, D. C. Biswas, R. K. Choudhury, D. M. Nadkarni, and A. Saxena, *Phys. Rev. C* **53**, R544(R) (1996).
- [67] R. G. Thomas, R. K. Choudhury, A. K. Mohanty, A. Saxena, and S. S. Kapoor, *Phys. Rev. C* **67**, 041601 (2003).
- [68] A. A. Sonzogno, R. Vandenbosch, A. L. Caraley, and J. P. Lestone, *Phys. Rev. C* **58**, R1873(R) (1998).
- [69] K. Nishio, H. Ikezoe, Y. Nagame, M. Asai, K. Tsukada, S. Mitsuoka, K. Tsuruta, K. Satou, C. J. Lin, and T. Ohsawa, *Phys. Rev. Lett.* **93**, 162701 (2004).
- [70] T. Døssing and J. Randrup, *Phys. Lett. B* **155**, 333 (1985).
- [71] B. Heusch, C. Volant, H. Freiesleben, R. P. Chestnut, K. D. Hildenbrand, F. Pühlhofer, W. F. W. Schneider, B. Kohlmeyer, and W. Pfeffer, *Z. Phys. A* **288**, 391 (1978).
- [72] D. J. Hinde, *Nucl. Phys. A* **553**, 255c (1993).
- [73] L. Donadille, E. Liatard, B. Benoit, F. Hanappe, L. Stuttge, G. Rudolf, E. M. Kozulin, Y. A. Lazarev, P. Desesquelles, L. A. Litnevsky, B. Bilwes, J. Bruandet, G. J. Costa, O. Dorvaux, F. Farget, J. Fayot, G. Guillaume, A. Huck, I. Itkis, M. G. Itkis *et al.*, *Nucl. Phys. A* **656**, 259 (1999).
- [74] F. Goldenbaum, M. Morjean, J. Galin, E. Liénard, B. Lott, Y. Périer, M. Chevallier, D. Dauvergne, R. Kirsch, J. C. Poizat, J. Remillieux, C. Cohen, A. L'Hoir, G. Prévot, D. Schmaus, J. Dural, M. Toulemonde, and D. Jacquet, *Phys. Rev. Lett.* **82**, 5012 (1999).
- [75] M. Morjean, A. Chbihi, C. Escano-Rodriguez, J. D. Frankland, C. Stodel, D. Jacquet, M. Laget, L. Tassan-Got, J. L. Charvet, R. Dayras, A. Drouart, L. Nalpas, C. Volant, A. L'Hoir, C. Cohen, M. Parlog, M. Chevallier, D. Dauvergne, R. Kirsch, P. Lattes *et al.*, *Phys. Rev. Lett.* **101**, 072701 (2008).
- [76] D. Jacquet and M. Morjean, *Prog. Part. Nucl. Phys.* **63**, 155 (2009).
- [77] M. O. Frégeau, D. Jacquet, M. Morjean, E. Bonnet, A. Chbihi, J. D. Frankland, M. F. Rivet, L. Tassan-Got, F. Dechery, A. Drouart, L. Nalpas, X. Ledoux, M. Parlog, C. Ciortea, D. Dumitriu, D. Flueraşu, M. Gugişu, F. Gramegna, V. L. Kravchuk, T. Marchi *et al.*, *Phys. Rev. Lett.* **108**, 122701 (2012).

- [78] R. Rafiei, R. G. Thomas, D. J. Hinde, M. Dasgupta, C. R. Morton, L. R. Gasques, M. L. Brown, and M. D. Rodriguez, *Phys. Rev. C* **77**, 024606 (2008).
- [79] C. J. Lin, R. du Rietz, D. J. Hinde, M. Dasgupta, R. G. Thomas, M. L. Brown, M. Evers, L. R. Gasques, and M. D. Rodriguez, *Phys. Rev. C* **85**, 014611 (2012).
- [80] K. Mazurek, P. Nadochy, E. Ryabov, and G. Adeev, *Eur. Phys. J. A* **53**, 79 (2017).
- [81] V. S. Ramamurthy and S. S. Kapoor, *Phys. Rev. Lett.* **54**, 178 (1985).
- [82] Y. Aritomo and M. Ohta, *Nucl. Phys. A* **753**, 152 (2005).